Journal of Macromolecular Science, Part A
Publication details, including instructions for authors and subscription information:
http://www.informaworld.com/smpp/title~content=t713597274

Preparation, Characterization and Cell Attachment Studies of Electrospun Multi-scale Poly(caprolactone) Fibrous Scaffolds for Tissue Engineering

K. T. Shalumon[a]; N. S. Binulal[a]; M. Deepthy[a]; R. Jayakumar[a]; K. Manzoor[a]; S. V. Nair[a]
[a] Amrita Center for Nanosciences and Molecular Medicine, Amrita Institute of Medical Sciences and Research Center, Amrita Vishwa Vidyapeetham University, Kochi, India

Online publication date: 19 November 2010

To cite this Article Shalumon, K. T. , Binulal, N. S. , Deepthy, M. , Jayakumar, R. , Manzoor, K. and Nair, S. V.(2011) 'Preparation, Characterization and Cell Attachment Studies of Electrospun Multi-scale Poly(caprolactone) Fibrous Scaffolds for Tissue Engineering', Journal of Macromolecular Science, Part A, 48: 1, 21 — 30
To link to this Article: DOI: 10.1080/10601325.2011.528288
URL: http://dx.doi.org/10.1080/10601325.2011.528288

Journal of Macromolecular Science, Part A: Pure and Applied Chemistry (2011) **48**, 21–30

ISSN: 1060-1325 print / 1520-5738 online
DOI: 10.1080/10601325.2011.528288

Taylor & Francis
Taylor & Francis Group

Preparation, Characterization and Cell Attachment Studies of Electrospun Multi-scale Poly(caprolactone) Fibrous Scaffolds for Tissue Engineering

K. T. SHALUMON, N. S. BINULAL, M. DEEPTHY, R. JAYAKUMAR*, K. MANZOOR and S. V. NAIR**

Amrita Center for Nanosciences and Molecular Medicine, Amrita Institute of Medical Sciences and Research Center, Amrita Vishwa Vidyapeetham University, Kochi, India

Received, Accepted June 2010

Electrospun nano, micro and micro/nano (multiscale) poly(caprolactone) (PCL) fibrous scaffolds with and without nano hydroxyapatite (nHAp) was prepared. All the scaffolds were evaluated for its spectroscopic, morphological, mechanical, thermal, cell attachment and protein adsorption properties. The cell attachment studies showed that cell activity on the nano-fibrous, as well as multi-scale scaffolds with and without nHAp was higher compared to micro-fibrous scaffolds. A time dependent cell attachment study on aligned micro-fibers was carried out to elucidate the difference in cell interaction on micro-fibers. The cell activity, proliferation and total protein adsorption on the nano-fibers/nano-fibers with nHAp was significantly higher than on the micro-fibers, although the adsorption per unit area was less on the nano-fibers due to the much higher surface area of nano-fibers. These results suggest that a combination of a micro- and nano-fiber hierarchical scaffold could be more beneficial for tissue engineering applications than the individual scaffolds provided the amount of nano- fibers could be suitably optimized.

Keywords: Tissue engineering, electrospinning, fibrous composite scaffold, hydroxyapatite, cell viability

1 Introduction

Tissue engineering is a promising field having the potential for providing replacement tissues and organs, an area of research established by the pioneering work of Langer and Vacanti in the 1990's (1). This field envisages combining cell, scaffold (initial structure for guided cell proliferation) and bioreactor technologies, towards the design and fabrication of neo-tissues/organs (2). A key to success here is to try and as closely as possible simulate the extracellular matrix (ECM) environment (3–5) so as to stimulate cell attachment and proliferation, as well as to improve the cell viability. It is well known that the ECM is neither a nano-scale nor a micro-scale structure, but instead is a hierarchical structure consisting of both micro and nano levels of scale. The micron scale structure potentially allows cell mobility because the pores in such a structure are large enough for cells to infiltrate through, while the nano structure allows for extensive protein-mediated interactions with cell membranes that have potential to improve cell viability and proliferation rates of cells. This study attempts to simulate the ECM with a juxtapositioning of nano- and micro-sized fibers of a biodegradable polymer within the same scaffold using electrospinning (6–14). It also examines in detail the nature of cell material interactions resulting from such a multi-scale structure.

A second aspect of importance that was considered was the local chemistry of the scaffold. HAp is a basic constituent of bone tissue, which forms during the mineralization step of bone formation. Since the presence of HAp (15) is known to aid in cell- material interaction favorably (16), we have examined the role of nHAp in conjunction with the multi-scale structure of the scaffold, in particular, to address the relative importance of structure vs. chemistry in bone tissue formation. In the present study, we have selected PCL, relatively inexpensive, highly elastic, thermoplastic polyester because of its lack of toxicity and slow degradation time (17). PCL has been reported for its biocompatibility and good mechanical properties in tissue engineering applications (18–21). In this paper, we report the processing, characterization and biological evaluation

*Address correspondence to: R. Jayakumar, Amrita Center for Nanosciences and Molecular Medicine, Amrita Institute of Medical Sciences and Research Center, Amrita Vishwa Vidyapeetham University, Kochi-682 041, India. Tel: +91-484-4008750; Fax: +91-484-2802030; E-mail: jayakumar77@yahoo.com and rjayakumar@aims.amrita.edu
**S. V. Nair, E-mail: shantinair@aims.amrita.edu

Table 1. Preparation of nano, micro, and multiscale fibers with or without HAp

Structure code	*Concentration of PCL/nHAP*	*Viscosity (cp) at 22°C*	*Fiber Type*	*Fiber Diameter (microns)*
A	Solution 1: 12wt % PCL in $CHCl_3/CH_3OH$	55	Nano	244.70 ± 18.81 nm
B	Solution 2: 30wt % PCL in $CHCl_3$	1 470	Microfibers	6.81 ± 0.39 μm
C	Solution 3: 12wt% PCL, +1.5 wt % (of PCL) HAp in $CHCl_3/CH_3OH$	74	Nano	269.54 ± 42.24 nm
D	Solution 4: 30wt% PCL+1.5 wt % (of PCL) HAp in $CHCl_3$	1722	Microfibres	11.31 ± 1.85 μm
E	Solution 1 + Solution 2	—	Micro + Nano fibers	Nano & Micro diameters unchanged
F	Solution 3 + Solution 4	—	Micro + Nano fibers	Nano & Micro diameters unchanged

of electrospun scaffolds of PCL for tissue engineering applications.

2 Experimental

2.1 Materials

PCL (M_W ~43000-50000) was purchased from Polysciences, Inc., USA. Methanol and chloroform (HPLC grade) was purchased from Qualigens, India. Calcium hydroxide and Ortho phosphoric acid were purchased from SD Fine India Ltd. All the chemicals used were as received, without further purification.

2.2 Synthesis and Characterization of nHAp

nHAp was prepared according to a procedure reported elsewhere (22). Briefly, 9.26 g of $Ca(OH)_2$ was added to 250 ml distilled water and stirred at 100°C for 2 h. 0.3 M of H_3PO_4solution was added dropwise to the above at a rate of ~ 2 mL/min. The addition of this acidic solution continued till the pH reached to 7.4. After the addition stopped, the reaction was allowed to proceed at 100°C for another 2 h, and then kept overnight at ambient. The supernatant was discarded and the precipitate was washed four times with hot water with subsequent centrifugation. The precipitate was dried overnight under vacuum at 60°C. The prepared nHAp was characterized for its crystallinity and particle size using X-ray diffractometry [Rigaku Dmax-C fitted with Cu-K_α ($\lambda = 1.541$ Å)] and Dynamic Light Scattering (DLS) technique [Nicomp 380, Particle Sizing Systems, USA] respectively. Spectroscopic evaluation of prepared fibrous scaffolds was carried out using a Fourier Transform Infrared Spectrometer (FTIR) [Perkin-Elmer Spectrum RX1] and the microscopic and EDS characterization by a JEOL analytical Scanning Electron Microscope (SEM) [JSM-6490 LA].

2.3 Preparation of Nano, Micro and Micro/nano- Fibrous PCL Scaffolds with and without nHAp

Nano, micro and micro/nano- fibrous PCL scaffolds with and without nHAp were prepared by the electrospinning technique. Viscosity of the polymer solutions as well as preparation conditions of nano, micro and micro/nano-fibrous PCL scaffolds with and without nHAp are shown in Table 1. The basis of the parameter selections was from a previous study (23) wherein the fiber diameter was shown to decrease as the factor eV/η increased. Here e is the solution charge per unit volume; V is the voltage applied and η the solution viscosity. A custom-designed electrospinning setup was fabricated using a high voltage DC power supply [Model RR30P, 0-30 kV, Gamma High Voltage Inc., USA], an infusion syringe pump [Model KDS 220, KD Scientific Inc., USA], 20 ml syringes with blunt ended metal needles [21 gauge, BD Sciences Ltd., Spain] and an aluminium plate collector or a grounded static and translational electrode as schematically represented in Figure 1. The sample solution was electrostatically drawn from the tip of the needle by applying a high voltage between the disk electrode and the collector. The flow rate of the solution, applied voltage, and distance between the needle tip and collector (air gap) were optimized. Nanofibers were obtained by electrospinning 12 wt% of the polymer solution in chloroform/methanol mixture (3:1) to the grounded metallic target, whereas for fabricating microfibers, 30 wt% PCL solution was used. The micro-/nanofibrous scaffold were fabricated using the corresponding optimized concentrations of PCL solutions for nano- and micro-fibers.

Composite fibers of nano and micro PCL were obtained by incorporating nHAp into identical concentrations of PCL solution. The composite nano-fibers were prepared by mixing 12 wt% PCL in chloroform/methanol (3:1) mixture containing 1.5 wt% nHAp. For preparing composite microfibers, 30 wt% of PCL was dissolved in chloroform with 1.5 wt% nHAp. nHAp was uniformly dispersed in chloroform/methanol mixture by sonication prior to the dissolution of PCL in this solvent system. All the solutions

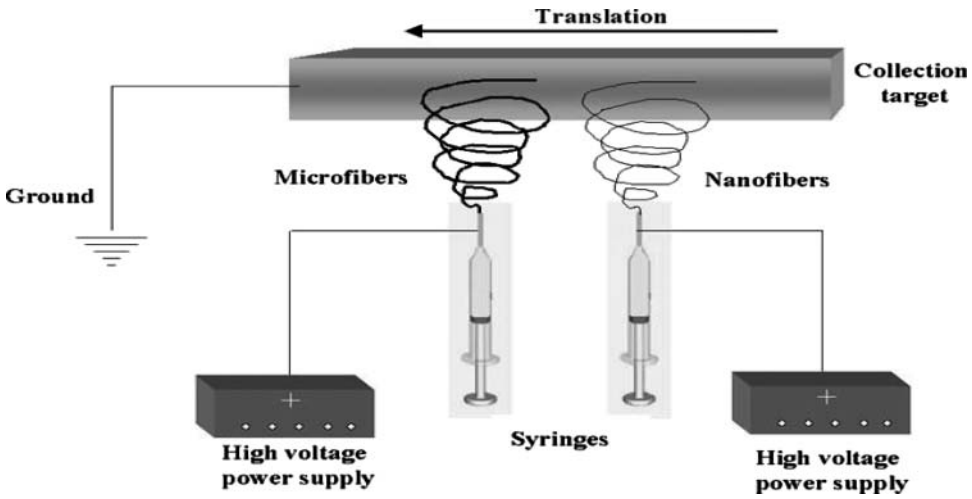

Fig. 1. Schematic diagram of one-step electrospinning set up.

were electrospun as stated earlier. For obtaining aligned micro-fibers with and without hydroxyapatite, the polymer solution was electrospun onto a rotating cylindrical mandrel (5000 rpm).

The electrospinning conditions for the preparation of different fibrous scaffolds are shown in Table 2. In the fabrication of micro/nano- fibrous scaffolds, two syringes were connected to two different high voltage power sources. This setup is an alteration of the one discussed in literature for preparing mixing/sequential electrospun fibers (24–26). In another study, Tuzlakoglu et al. (27) has created micro-nano fibers by impregnating the micro-fiber scaffold with nano-fibers by moving a micro-fibrous scaffold through electrospun nano-fiber jets. In our study, micro-fibers were electrospun continuously from one syringe onto a grounded stage that was translated at an optimal speed of ~6 cm/min, while nano-fibers were electrospun intermittently from the second syringe (nano-fibers were spun for 12% of the time). The translation was provided such that the polymer fibers were spun in an interwoven fashion. The resultant matrix yielded micro-/nano-fibrous scaffold geometry. The volume of nano-fibers was calculated to be 2.5% of that of the micro-fibers based on experimental flow rates, concentration of PCL and electrospinning time. SEM images were utilized to analyze the pore size distribution in each scaffold. An average of the minimum and maximum pore dimensions of at least 25 pores in the electrospun mat was used for the analysis.

2.4 Characterization of the Electrospun Scaffolds

2.4.1. *FTIR*

Infrared Spectroscopy was employed to confirm the presence of nHAp in the electrospun PCL scaffolds. For this, nHAp, PCL, PCL nanofibers and microfibers with nHAp were analyzed separately using FTIR in the range between 4000 and 400 cm^{-1}, with a resolution of 2 cm^{-1}.

2.4.2. *Thermal Studies*

Thermal stability of all the electrospun scaffolds was examined using SII model EXTAR TG/DTA 6200. All the samples were cut into small pieces pre-weighed and allowed to undergo programmed heating at a rate of 10°C/min.

2.4.3. *Mechanical Characterization*

The details of the mechanical studies are following. The samples were prepared with the following dimensions: length 25 mm and breadth 5 mm. A double-sided tape was glued to the top and bottom sides of the electrospun fibers to avoid damage to the fibers. The specimen thicknesses were measured using a digital gauge micrometer. The

Table 2. Conditions for preparation of different fibrous scaffolds

Structure code	*Fiber type*	*Flow rate (mL/h)*	*Voltage (kV)*	*Tip-target distance (cm)*
A	Nanofibers	1	10	10
B	Microfibers	1	8	10
C	Nanofibers with nHAp	1	10	10
D	Micro fibers with nHAp	1	8	10
E	Micro + Nano fibers*		8 (micro)/10 (nano)	10
F	Micro + Nano fibers with nHAp*	1	8 (micro)/10 (nano)	10

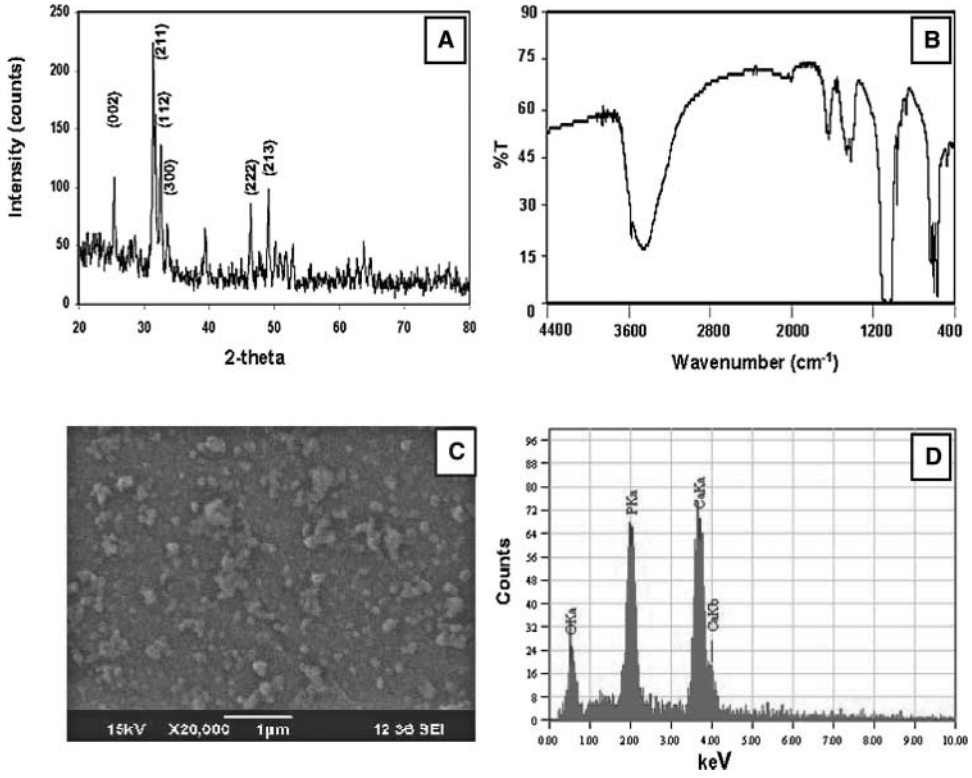

Fig. 2. (A) XRD pattern of nHAp (B) FTIR spectrum of nHAp (C) SEM of nHAp (D) EDS of nHAp.

tensile testing was performed using ORIENTEC Universal testing machine STA-1150 RTC with a crosshead speed of 3 mm/min (28). The recorded data were used to assess the maximum stress with respect to each fiber system.

2.5 Protein Adsorption

Adsorption of proteins on the developed scaffolds was measured using the standard Bicinchonic Acid assay. Briefly, pre-weighed scaffolds were incubated in serum containing cell culture media (MEM with 10% FBS) for 1 h and 6 h in a CO_2 incubator. After incubation, scaffolds were washed 3 times in PBS and the adsorbed proteins were eluted using elution buffer (chaps 0.5 wt% and SDS 10 wt%). The amount of adsorbed proteins on the fibrous scaffolds was quantified spectrophotometrically (Biorad).

2.6 Cell Attachment and Proliferation

The suitability of electrospun PCL scaffolds for cell attachment and proliferation was determined using the human osteoblastic cell line, MG63. All the scaffolds were ethanol/UV sterilized for 24 h and were seeded with cells (2.5×10^4 cells/3.6 cm^2) on 12-well plates. Cell attachment on non-woven nano, micro and nano/micro-enmeshed fibers as well as their nHAp-incorporated counterparts was qualitatively analyzed using SEM at 12 h. Cell proliferation on these scaffolds was quantitatively estimated using MTT assay (29) at 12 and 96 h. Cell attachment and spreading on aligned microfibers with and without nHAp was observed for six time points, viz., 1, 4, 12, 24, 72 and 96 h.

2.7 Statistical Analysis

All biological quantitative results were obtained from triplicate samples. Data was expressed as the mean ± SD and statistical analysis was carried out using student's *T*-test. A value of $p < 0.05$ was considered to be statistically significant.

3 Results and Discussion

3.1 Characterization of nHAp

HAp nanoparticles synthesized for preparing PCL composite fibers revealed good crystallinity as is evident from the XRD spectrum in Figure 2A (JCPDS data file no. 090432). Figure 2B gives the FTIR spectrum of nHAp. The vibration of hydroxyl group appearing at 3571 and 633 cm^{-1} and the phosphate stretching vibration observed at 1031, 1094 and 963 cm^{-1} are the characteristic features of hydroxyapatite. The phosphate bending vibrations of nHAp are observed in the spectrum at 603 and 565 cm^{-1} (30). A typical scanning electron micrograph of nHAp is given in Figure 2C, which reveals that the nanoparticles are

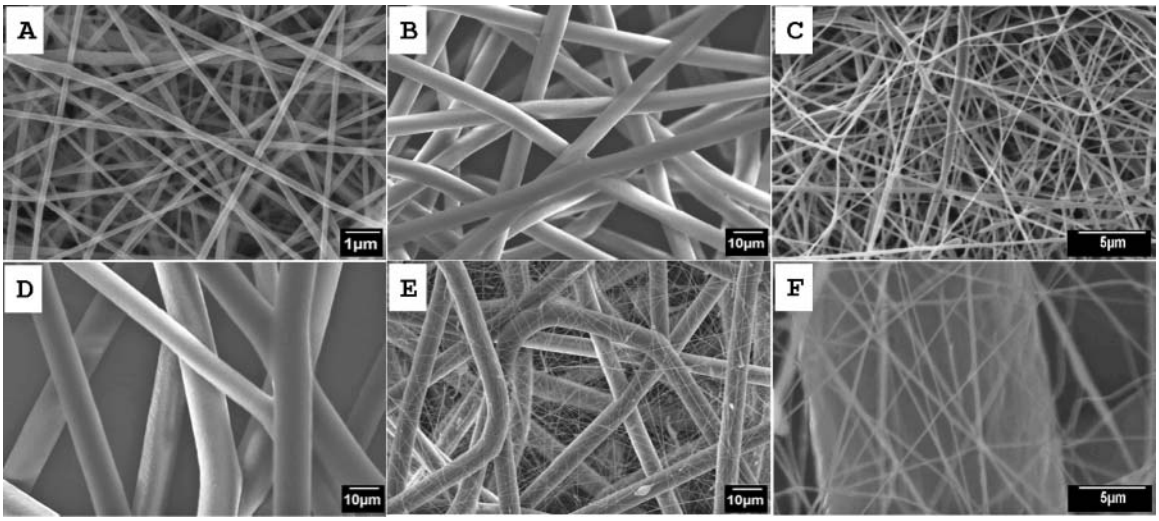

Fig. 3. SEM of electrospun PCL (A) Nano-fibers; (B) Micro-fibers; (C) Nano-fibers with nHAp; (D) Micro-fibers with nHAp; (E) Multi-scale fibers; (F) Multi-scale fibers with nHAp.

nearly monodispersed and spherical in shape, with an approximate particle size of 80 nm. The particle size evaluated from SEM is comparable with the particle size of $\sim 89 \pm 4$ nm obtained from DLS measurements. EDS of nHAp particles is given in Fig. 2D and it represents a Ca/P ratio of 1.7, which compares well with the theoretical value (1.67) of nHAp (22).

3.2 Fiber Morphology

Various processing parameters such as viscosity, solvent nature, applied voltage, flow rate, tip-target distance and needle diameter critically influence the fiber morphology during electrospinning. The conditions for obtaining nanofibers such as higher dielectric constant of the solution (because of the presence of methanol in chloroform), higher applied voltage and lower viscosity would be expected to yield the smallest fiber diameter. Representative SEM images depicting the fiber morphology and size distribution of the prepared nano- and micro-fibers are shown in Figures 3A and B respectively. Figure 3C and D are the SEM images of the corresponding nano- and micro-fibers containing nHAp. The SEM images clearly revealed that all the fibers had smooth morphology and uniform shape. The fiber diameter values shown in Table 1 indicate micro fibers have an average diameter of 6.2 μm and nano-fibers of 248 nm.

It should be noted that incorporation of nHAp did not alter the shape of the fibers. Nano- as well as the microfiber diameters increased after nHAp incorporation. This is attributed to the increased viscosity of the polymer solution after nHAp incorporation (Table 1). Figure 3E and F represent the SEM images of micro-/nano- fiber scaffold and micro-/nano- fiber scaffold with nHAp. The morphology and diameter of nano- and micro- fibers in the enmeshed system was the same as that of the pure nano- and micro- fiber systems. The pore size distributions of each scaffolds measured using SEM was indicative of the suitability of the scaffold for tissue engineering. Pore sizes need to be larger than cell sizes (10–30 microns) to allow for cell access to the scaffold interiors. For nano- and microfibers, the pore size measured was 2.32 ± 0.63 μm and 27.04 ± 6.19 μm respectively. The pore size for nHAp-incorporated scaffolds was 1.85 ± 0.43 μm for nano-fiber and 23.36 ± 6.77 μm for micro-fiber, respectively. The reduction in pore sizes for nano- and micro-fibers with nHAp compared to their corresponding counterparts without nHAp is attributed to the increased fiber diameters of the scaffolds upon incorporation of nanoparticles. In multiscale scaffold, the amount of nano- fibers is 2.5% by volume, which would help to maintain the porosity of microfibers.

3.3 FTIR Evaluation of Fibrous Scaffolds

Figure 4(i) (A–D) represent the FTIR spectra of pristine PCL, nHAp and PCL nano-fibers and micro-fibers containing nHAp, respectively. From Figure 4(i) (A), the peaks at 2810 and 1723 $cm^{-1}$are characteristics of C-H and C=O vibrations of PCL. The nHAp spectrum shown in Figure 4 (i) (B) represents the absorption bands at 565 and 603 cm^{-1}, which are characteristic of the phosphate bending vibrations of nHAp. The FTIR spectra of PCL nano- and micro-fibers with nHAp (Figure 4(i) C and 4(i) D) (22) depict all the characteristic peaks of PCL and nHAp, thereby confirming the distribution of nHAp in the composite fibers.

Table 3. Mechanical testing of different types of polymeric scaffolds

	Nanofiber	*Microfiber*	*Microfiber/ Nanofiber*	*Nanofiber nHAp*	*Mircrofiber*	*Microfiber/ Nanofiber/nHAp*
Stress (M Pa)	1.85 ± 0.14	1.35 ± 0.18	1.72 ± 0.12	1.12 ± 0.19	1.56 ± 0.17	1.69 ± 0.12
Strain (%EL)	34.8	21	123	13.1	66.0	117

3.4 Thermal Studies

Figure 4(ii) (A) represents the DTA curve of the prepared scaffolds. In DTA, all the electrospun scaffolds showed similar endothermic transition behavior. However, nanofibers with nHAp showed a slightly enhanced melting point at 66°C compared to the normal melting point of PCL at 63°C. The other endothermic transition values (melting point) of nano, micro, micro/nano, micro/HAp, micro/nano/Hap fibers are respectively 64.3, 63.4, 64.2, 64 and 64.1°C. This may be due to the presence of nHAp in the nanofibers, which increases the thermal withstanding capacity of the fibers by increasing the initial melting point of the composite fibers (31). Figure 4(iii) shows the TGA curve of prepared scaffolds. A similar trend was observed for the decomposition behavior of different scaffolds, but with slightly enhanced initial decomposition temperature (IDT) for nanofibers with nHAp (370°C). This may be due to the uniform dispersion of nHAp in the fibers, which hinders the decomposition of PCL (32).

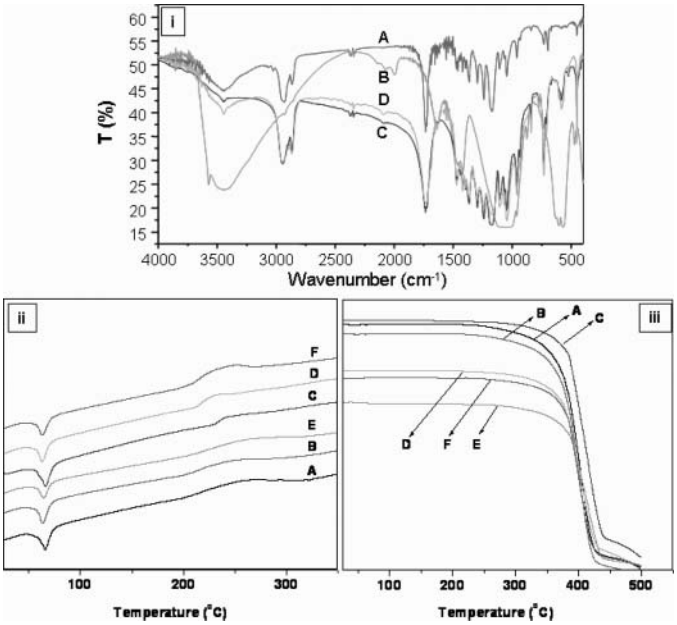

Fig. 4. (i) FTIR spectrum of electrospun scaffolds: (A) pristine PCL (B) pristine nHAp (C) nano-fibers with nHAp (D) microfiber with nHAp and (ii and iii) DTA and TGA curves of electrospun scaffolds: (A) Nanofibers (B) Microfibers (C) Nanofibers with nHAp (D) Microfibers with nHAp (E) Micro/nano fibers (F) Micro/Nano fibers with nHAp.

3.5 Mechanical Studies

The mechanical stability of each scaffold type is given in Table 3. All the composite fibers except nanofibers with nHAp showed more strength compared to the respective bare fibers. Among fibers without nHAp, nano-fibers measured to have more strength (1.85 ± 0.14) than the micro/nano (1.72 ± 0.12) or micro-fibers (1.35 ± 0.18). In the case of composite nanofibers, a lower mechanical stability was observed when compared to bare nanofibers (33, 34). This is due to the increased brittle nature in nanofibers with nHAp compared to nanofibers alone. But in the case of microfibers, mechanical strength of the fiber had direct effect in nHAp incorporation. This is due to the lesser unit density of microfibers with nHAp, which is below the optimum filler concentration, compared to nanofibers/nHAp, and hence, reduces the brittle character of the micofiber/nHAp scaffold. This relationship between brittleness and mechanical strength of nano and microfibers with and without nHAp can also be attributed to the strain behavior. However, for micro/nano fibers, the presence of nanofibers embedded in the micro-fiber matrix would be the cause for their increased mechanical strength, in comparison to the microfibers alone. In the case of percentage elongation, all the nano and micro fibrous scaffolds with and without HAp exhibited relative low strain values. But for micro/nano fibers the strain values where comparatively higher than corresponding nano or micro fibers. This might be due to the cumulative elongation effect when nano and micro fibers

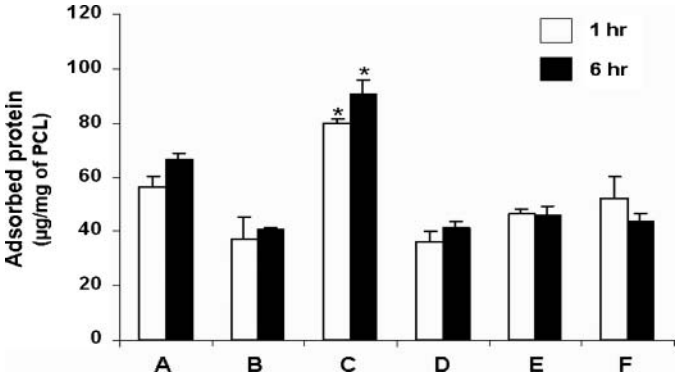

Fig. 5. Total protein adsorption on different scaffolds (A) Nanofibers; (B) Microfibers; (C) Nanofibers with nHAp; (D) Microfibers with nHAp; (E) Micro/nano fibers; (F) Micro/nano fibers with nHAp. *Significant difference ($p < 0.05$) compared with other pristine or nHAp incorporated fibers.

were enmeshed together. Further studies are underway to evaluate the optimum concentration nHAp in fibrous scaffolds with maximum strength.

3.6 Protein Adsorption Studies

The total protein adsorption was significantly higher on nano-fibrous scaffolds compared to micro and micro/nano scaffolds (Fig. 5). At 1 h, the adsorption on nanofibers was comparatively lesser than that on 6 h. This elevated value in adsorption is attributed to high surface to volume ratio of nanofibers. In the case of nHAp incorporated fibers, nanofibers with nHAp shows more adsorption at 6 h compared to all other scaffolds with and without nHAp. We also demonstrated that nanofibers will have maximum protein adsorption at 6 h and further incubation leads to desorption of proteins from the surface of fibers (35). As per Equation 1, when nanoparticles are present, due to the high surface to volume ratio, more number of nHAp will be present on the surface of the fibers and this would be the reason for maximum protein adsorption for nanofibers with nHAp (36).

In the case of protein adsorption per unit area, the question that needs to be addressed is whether the higher protein content is proportionate with the higher available surface area in the nano-fibrous scaffold. Protein adsorption was measured for the same weight, w, of each scaffold type. If the density of PCL is ρ, then the actual fiber volume is w/ρ. The surface area per unit volume of the fibers of length L is $2\pi RL/\pi R^2L = 2/R$. Therefore the total actual fiber surface area in the weight, w, is $(w/\rho)(2/R)$. This shows that the maximum surface coverage (in terms of the weight of protein per unit fiber surface area) will be very small on nano-fibers compared to that on the micro-fibers even though the total protein content is much higher on the nano-fibers. Clearly, this follows from the fact that the surface area is much higher for nanofibers. One possible explanation for the smaller protein coverage is that the protein desorption rate constant for the surface is higher for the nano-fibers compared to the micro-fibers. This also very well explained in our previous study (35). As given by the Langmuir theory, the net rate of protein adsorption, r_A can be given by:

$$r_A = k_A C_b (1 - \Theta) - k_D \quad (1)$$

Where, k_A, k_D are respectively the adsorption and desorption rate constants, C_b is the bulk protein concentration and Θ is the surface protein coverage. When k_D increases relative to k_A, the equilibrium surface coverage of protein decreases. The much lower value of the protein on the nano-fibers compared to the available area suggests that PCL nano-fibers may have lower values of (kA/kD) for proteins than for the micro-fibers.

3.7 Cell Attachment Studies

The cells that attached to the nano-scaffold at 12 h of incubation spread and formed a layer above the nano-fibers as seen in Figure 6A. In contrast, cells on the micro-scaffold showed a globular morphology and minimum lateral spreading (Fig. 6B) after the same time. The cells grown on nHAp incorporated composite PCL nano-scaffold exhibited a flat morphology with slightly higher spreading than on pristine scaffolds (Fig. 6C). These observations

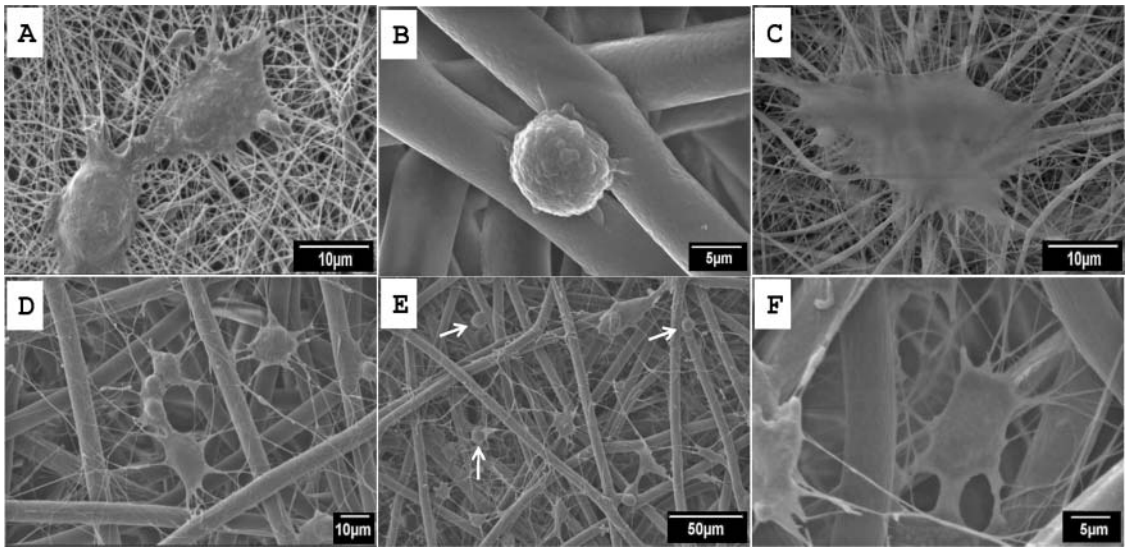

Fig. 6. Typical SEM of cell attachment after 12 h of incubation (A) Flat morphology of cells attached on nano-fibrous scaffold; (B) Globular morphology of cells attached on micro-fibrous scaffold; (C) Cells grown on nHAp incorporated nano-fibrous scaffold; (D) Cells grown on multi-scale scaffold; (E) Cell growth into the multisacale scaffold–arrows indicate spherical morphology of cells attached to micro-fibers; (F) Cell access to the interior of the multi-scale scaffold through the pores in the micro-fibers.

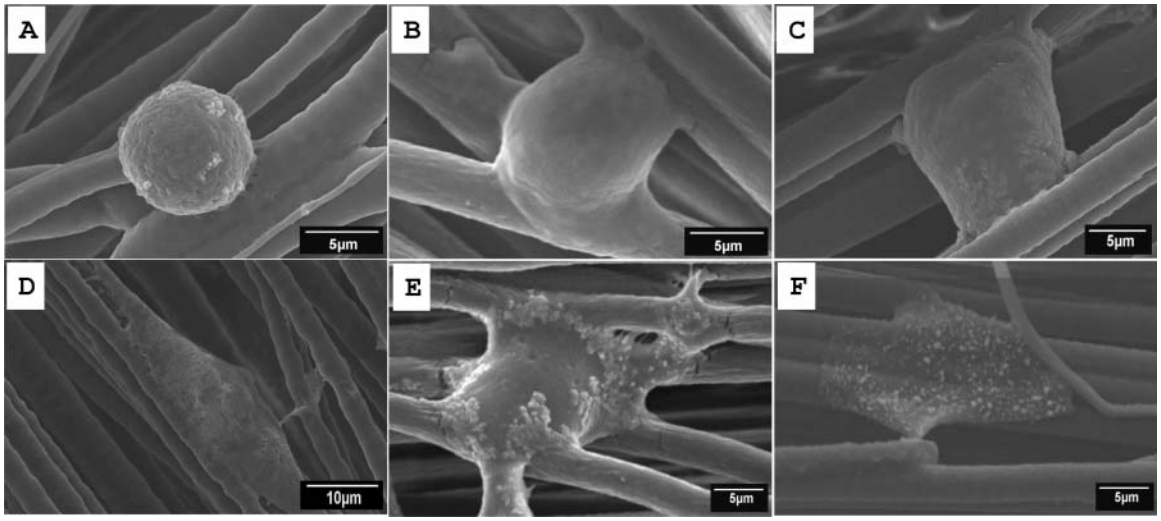

Fig. 7. Typical SEM of time-dependent cell attachment on aligned micro-fibers for (A) 1; (B) 4; (C) 12; (D) 24; (E) 72 and (F) 96 h.

indicate a dramatic difference in cell behavior when exposed to fiber geometries. Nano-fibers appear to show a significant disposition towards initiating cell attachment and spreading unlike micro-fiber geometries. It has been reported that the cell interaction with specific materials is strongly mediated by the prior attachment of specific proteins on such surfaces (13, 37). Our previous study (38) has also shown that on titania nanostructured surfaces, adsorption of specific adhesion proteins is significantly higher. Our separate study (35) of protein adsorption on micro- vs. nano-fibers has shown that the total protein adsorbed as well as the adsorption of specific adhesion proteins on nano- fibers was considerably higher than on micro-fibers. This supports the role of prior protein adsorption differences on nanofibers and nanofibers with nHAp compared to microfibers and microfibers with nHAp, as being responsible for the dramatic differences seen in this study.

Supporting the observation on nano- and micro- fiber scaffolds individually, when cells were seeded onto a multiscale scaffold, a striking difference between the cell morphology associated with the two fiber size regimes was found. Cells attached to the micro-fibers remained globular as in the case of a bare micro-fibrous scaffold, whereas the cells that attached to the nano-fibers within the multiscale scaffold were laterally stretched and extended as in the case of nano-fibers alone. This can be clearly seen in Figure 6D, E and F. Arrows indicate the globular morphology of cells on micro-fibers. Tuzlakoglu et al. (27) also observed that when both nano- and micro-fibers are present, the cells attach primarily to the nano- fibers and are consistent with our results.

3.8 Time-dependent Studies of Cell Morphology

The morphology of cells on nanofibers and microfibers are not too different for a longer period of cell attachment, that is, if the cells spread very slowly on the micro fibers compared to that on nano-fibers, then one would observe rounded morphology of the cells on micro-fibers and flat morphology on nano-fibers. However, at long periods of time, both size regimes should exhibit a relative flat spread structure. To test the hypothesis, we used aligned micro fibers to evaluate the cell adhesion. Randomly oriented micro-fibers had large pores that the cells would easily fall through it so that it was difficult to make the cell morphology study. The aligned micro-fibers were obtained by electrospinning onto a rotating mandrel giving a scaffold structure with little porosity.

SEM images representing the cell attachment on the aligned microfibers with and without nHAp at various time points, viz., 1, 4, 12, 24, 72 and 96 h are depicted as A, B, C, D, E and F in Figures 7 and 8, respectively. After 1 h, both sets of micro-fibers showed almost globular cell morphology (Fig. 7A and 8A) suggesting weak attachment to the scaffolds. The delay in cell spreading continued for several hours (Fig. 7B and C and Fig. 8B and C). Figures 7D and 8D show the initiation of cell spreading at 24 h. The cells started spreading over neighboring fibers along the fiber axis after 72 h (Fig. 7E and 8E) and finally attained a flattened morphology at $\sim$ 96 h (Figs. 7F and 8F). In contrast, the cell spreading appeared to be much more rapid in a nano-fibrous scaffold, with complete lateral spreading observed at the 12 h point (Fig. 6A). More work at time intervals less than 12 h would be needed to reveal the time point, wherein cells became fully spread in the nano-fiber scaffold.

3.9 MTT Assay

The results of the MTT assay for the metabolic activity of cells (39, 40) after 12 and 96 h of exposure is shown in Figure 9. After 12 h, the metabolic activity was essentially

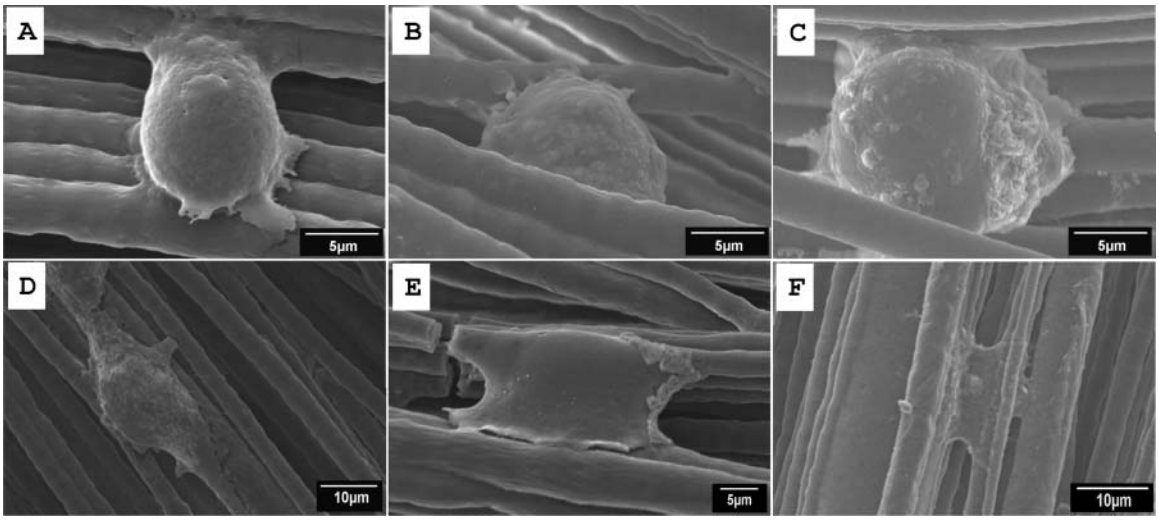

Fig. 8. Typical SEM of time-dependent cell attachment on aligned micro-fibers with nHAp for (A) 1; (B) 4; (C) 12; (D) 24; (E) 72 and (F) 96 h.

the same on all scaffold types but after 96 h, there are distinct differences between the different scaffolds. Nano scaffolds show better activity than micro scaffolds. Similarly, the activity on the multi-scale scaffold is higher than on the micro scaffold alone. Since the cells are primarily attaching to the nano-fibers and spreading well by this process, the presence of the nano-fibers can be expected to improve cell viability, consistent with the MTT results.

The addition of nHAp to the nano scaffold improved the cell activity significantly. The addition of nHAp slightly improved cell activity in the micro and multi-scale scaffold. The influence of nHAp can be explained on the basis of the percentage of nHAp that is present on the surface of fibers. When micro scaffolds are dipped in nHAp, the functionality of nHAp may be high, but in our case, the nHAp was added to the electrospinning solution and hence, are dispersed within the fibers. If the fiber radius is R and the nHAp radius is r,the nHAp present in a layer of thickness r on the surface can be considered to have surface activity or be exposed. Hence, the fraction, f, of nHAp that is exposed on the fibers can be given by:

$$f = 2\left(\frac{r}{R}\right) - \left(\frac{r}{R}\right)^2 \tag{2}$$

when R $\gg$ r, there are very few HAp particles on the fiber surface. When R approaches r the fraction approaches unity, that is, all of the nHAp is on the surface. In our case, for the microfibers r = 0.013 R, whereas for the nano-fibers r = 0.33 R. As a result, 55% surface exposure of the nHAp in the nano-fibers and only 2.6% surface exposure for the microfibers. This is very likely the reason why cell activity in the micro and multi-scale scaffolds were not affected much by nHAp additions. In the multi-scale scaffold, the nanofibers were only 2.5% by volume and hence, nHAp probably did not play a significant role in cell metabolic activity in that scaffold. However, the multi-scale scaffold was still superior to the micro scaffold alone and more studies are needed to optimize the amount of nHAp needed.

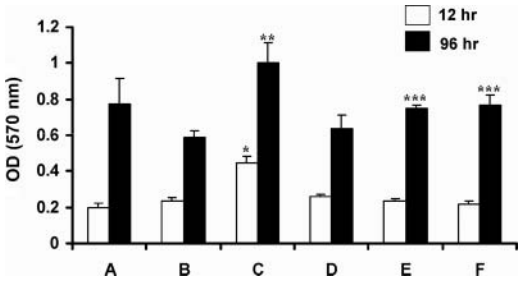

Fig. 9. The human osteoblastic cells were seeded on various scaffolds as indicated and cell proliferation was measured at 12 and 96 h using MTT assays as described in methods. Data represent the samples analyzed in triplicates. *Significant difference ($p < 0.05$) compared with other pristine or nHAp incorporated scaffolds at 12 h of incubation; **significant difference ($p < 0.05$) compared with nano-fiber scaffold; ***significant differences ($p < 0.05$) compared with micro-fiber scaffold or micro-fiber scaffold incorporated with nHAp.

4 Conclusions

Poly(caprolactone) nanofibers, microfibers and multi-scale fibers with and without nHAp were produced by electrospinning and were characterized. Mechanical and thermal studies reveal that nano-scale fibers are superior to microfibers. Protein adsorption study shows that nanofibers with nHAp show higher adsorption than other fibers at 6 h. Cells in the nano scaffold attached and spread rapidly on the nano- fibers, whereas the cell spreading process was

much slower in the micro-fibers. In the multi-scale scaffold, the small amount of nano-fibers was adequate to cause a substantial effect on cell attachment and proliferation. Although the multi-scale scaffold did not show more cell activity than nano scale scaffold, its cell activity was better than that of the micro-scale scaffold. The incorporation of nHAp into the nanofibrous scaffold enhancing the cell attachment, as well as protein adsorption was due to the high surface activity of nHAp. However, incorporation of nHAp into the micro-fibers did not affect the cellular activity. The composite scaffold with multi-scale geometry is an excellent system for tissue engineering.

Acknowledgements

The authors are grateful for the support of this work by the Department of Science and Technology, Government of India, through the National Nanoscience and Nanotechnology Initiative under the monitorship of Professor C. N. R. Rao. The authors K. T. Shalumon and N. S. Binulal are thankful to the Council of Scientific and Industrial Research (CSIR), Govt. of India for awarding the Senior Research Fellowship (SRF). The authors are also grateful to Professor Hiroshi Tamura for his help in mechanical studies and Mr. Sajin P. Ravi for his help in SEM measurements.

References

1. Langer, R. and Vacanti, J.P. (1993) *Science*, 260 (5110): 920–926.
2. Vacanti, C.A. (2006) *Tissue. Eng*., 12(5): 1137–42.
3. Liang, D., Hsiao, B.S. and Chu, B. (2007) *Adv. Drug Deli. Rev*., 10(59): 1392–12.
4. Mo, X.M., Xu, C.Y., Kotaki, M. and Ramakrishna, S. (2004) *Biomaterials*, 25(10): 1883–1890.
5. Venugopal, J., Low, S., Choon, A.T. and Ramakrishna, S. (2008) *J. Biomed. Mater. Res. B. Appl. Biomater*., 84(1): 34–48.
6. Li, W.J., Laurencin, C.T., Caterson, E.J., Tuan, R.S. and Ko, F.K. (2002) *J. Biomed. Mater. Res.*, 60(4): 613–621.
7. Yang, S., Leong, K.F., Du, Z. and Chua, C.K. (2002) *Tissue. Eng*., 8(1): 1–11.
8. Barnes, C.P., Sell, S.A., Boland, E.D., Simpson, D.G. and Bowlin, G.L. (2007) *Adv. Drug. Deli. Rev.*, 59(14): 1413–1433.
9. Chen, M., Patra, P.K., Warner, S.B. and Bhowmick, S. (2007) *Tissue. Eng*., 13(3): 579–587.
10. Yoshimoto, H., Shin, Y.M., Terai H. and Vacanti J.P. (2003) *Biomaterials*, 24(21): 2077–2082.
11. Ma, Z., Kotaki, M., Inai, R. and Ramakrishna, S. (2005) *Tissue. Eng*., 11(1–2): 101–109.
12. Yang, F., Murugan, R., Wang, S. and Ramakrishna, S. (2005) *Biomaterials*, 26 (15): 2603–2610.
13. Ballard, J.D., Dulgar-Tulloch, A.J. and Siegel, R.W. (2006) *Wiley Encyclopedia of Biomedical Engineering*, 4: 2489–2507.
14. Rutledge, G.C. and Fridrikh, S.V. (2007) *Adv. Drug. Del. Rev*., 59(26): 1384–1391.
15. Wutticharoenmongkol, P., Sanchavanakit, N., Pavasant, P. and Supaphol, P. (2005) *Macromol. Biosci*., 6(1): 70–77.
16. Huanan, W., Yubao, Li., Yi, Z., Jihua, Li., Sansi, Ma. and Lin, C. (2007) *Biomaterials*, 28(22): 3338–3348.
17. Zeng, J., Chen, X., Liang, Q., Xu, X. and Jing, X. (2004) *Macromol. Biosci*., 4(12): 1118–1125.
18. Causa, F., Netti, P.A., Ambrosio, L., Ciapetti, G., Baldini, N., Pagani, S., Martini, D. and Giunti, A. (2006) *J. Biomed. Mater. Res. Part A*., 76(1): 151–162.
19. Park, H., Cannizzaro, C., Vunjak-Novakovic, G., Langer, R., Vacanti, C.A. and Farokhzad, O.C. (2007) *Tissue. Eng*., 13(8): 1867–1877.
20. Pham, Q.P., Sharma, U. and Mikos, A.G. (2006) *Tissue. Eng*., 12(5): 1197–1211.
21. Xu, C., Inai, R., Kotaki, M. and Ramakrishna, S. (2004) *Tissue. Eng*., 10(7–8): 1160–1168.
22. Prakash, K.H., Ooi, C.P., Kumar, R., Khor, K.A. and Cheang, P. (2006) *IEEE Conference*, 10: 345–349.
23. Sajeev, U.S., Anoop, A.K., Deepthy, M. and Nair, S.V. (2008) *Bull. Mater. Sci*., 31: 343–351.
24. Kwon, I. K., Kidoaki, S. and Matsuda, T. (2005) *Biomaterials*, 26(18): 3929–3939.
25. Kidoaki, S., Kwon, I.K. and Matsuda, T. (2005) *Biomaterials*, 26(1): 37–46.
26. Rafael,G., Bjoern, B., Andreas, L. and Hans, G.B. (2009) *Macromol. Biosci*., 31(1): 59–64.
27. Tuzlakoglu, K., Bolgen, N., Salgado, A.J., Gomes, M.E., Piskin, E. and Reis, R. L. (2005) *J. Mater. Sci: Mater. Med.*, 16:1099-1104.
28. Zonggang, C., Bo, W., Xiumei, M., Lim, C.T., Ramakrishna, S. and Fuzhai, C. (2009) *Mater. Sci. and Eng-C*, 29 (8): 2428-2435.
29. Badami, A.S., Kreke, M.R., Thompson, M.S., Riffle, J.S. and Goldstein, A.S. (2006) *Biomaterials,* 27(4): 596–606.
30. Madhumathi, K., Binulal, N.S., Nagahama, H., Tamura, H., Shalumon. K.T., Selvamurugan, N., Nair, S.V. and Jayakumar, R. (2009) *Int. J. Biol. Macromol*., 44(1): 1–5.
31. Sotirios, P., Marras, K., Konstantina, T., Ioannis, Z., Ioannis, and Costas, P. (2008) *Acta Biomater*., 4(3): 756–765.
32. Avella, M., Bondioli, F., Canillo, V., Pace, E.D., Errico, M.E., Ferrari, A.M., Focher, B. and Malinconico, M. (2006) *Comp. Sci. Techn*., 66(7): 886–894.
33. Jongman, L., Giyoong, T., Young, H.K., In, S.P., Sang, H.K. and Soo, H.K. (2008) *Biomaterials*, 29(12): 1872–1879.
34. Sui, G., Yang, X., Mei, F., Hu, X., Chen, G. and Deng, X. (2007) *J. Biomed. Mat. Res. A*., 82(2)**:** 445–454
35. Binulal, N.S., Deepthy, M., Selvamurugan, N., Shalumon, K.T., Suja, S., Mony, U., Jayakumar, R. and Nair, S.V. (2010) *Tissue. Eng. Part A*., 16(2): 392–404.
36. Moncy, V.J., Vinoy, T., Yuanyuan, X., Susan, B., Elijah, N. and Derrick, D. (2010) *Macromol. Biosci*., 10(4): 433–444.
37. Ganesan, B. and Webster, T.J. (2006) *J. Mat. Chem*., 16(38): 3737–3745.
38. Divyarani, V.V., Manzoor, K., Deepthy, M., Selvamurugan, N. and Nair, S.V. (2009). *Nanotechnology,* 20(19): 195101–195112.
39. Kakoli, D., Susmita, B. and Amit, B. (2007) *Acta Biomater.,* 3(4): 573–585.
40. Sailaja, G.S., Ramesh, P., Kumary, T.V. and Varma, H.K. (2006) *Acta Biomater*., 2 (6): 651–657.